Journal of Science and Transport Technology
Journal homepage: https://jstt.vn/index.php/en

Nonlinear dynamic thermal buckling behavior of FG-GPLRC spherical shells and circular plates with porous core

Nguyen Thi Phuong[1,2], Vu Minh Duc[3,*], Vu Hoai Nam[4]
[1]Laboratory of Advanced Materials and Structures, Institute for Advanced Study in Technology, Ton Duc Thang University, Ho Chi Minh City, Vietnam
[2]Faculty of Civil Engineering, Ton Duc Thang University, Ho Chi Minh City, Vietnam
[3]Institute of Transport Technology, University of Transport Technology, Hanoi, Vietnam
[4]Faculty of Civil Engineering, University of Transport Technology, Hanoi, Vietnam

Article info
Type of article:
Original research paper

DOI:
https://doi.org/10.58845/jstt.utt.2024.en.4.4.43-54

***Corresponding author:**
Email address:
ducvm@utt.edu.vn

Received: 19/9/2024
Revised: 10/12/2024
Accepted: 12/12/2024

Abstract: A semi-analytical approach for dynamic buckling of sandwich functionally graded graphene platelet-reinforced composite (FG-GPLRC) spherical shells and circular plates under dynamic thermal loads with porous core is reported in the present research. Based on the higher-order shear deformation theory (HSDT), the formulations are established, and the large deflection nonlinearity of von Karman with the visco-elastic model of the nonlinear foundation is applied. The structure's nonlinear equations of motion can be obtained utilizing the Euler-Lagrange equations combined with Rayleigh dispersion functions. The dynamic thermal load is assumed to be a linear function of time. Numerical studies are investigated employing the Runge-Kutta method to obtain the dynamic thermal behavior, and the dynamic criterion of Budiansky-Roth can be used to determine the critical buckling temperature. Significant remarks on the dynamic thermal behavior of structures are presented through the investigated examples.

Keywords: Nonlinear dynamic thermal buckling; Porous core; The nonlinear viscoelastic foundation; The higher-order shear deformation theory (HSDT); Euler-Lagrange equations; Rayleigh dispersion functions.

1. Introduction

Spherical shells and circular plates are popularly utilized for different structures in engineering fields. Due to their popularity in application, various problems for these structures including static and dynamic nonlinear and linear buckling, and vibration responses are also of interest to many researchers.

In the last three decades, functionally graded material (FGM) with its superior advantages over classical composite materials has attracted the attention of many researchers to the static and dynamic problems of FGM shells and plates. Based on first-order shear deformation plate theory (FSDT), the thermal and mechanical axisymmetric buckling problems of FGM circular plates were studied by Najafizadeh and Hedayati [1]. The thermal buckling [2, 3] and vibration [2] problems of FGM circular plates were investigated by utilizing a finite element formulation. FGM spherical shells

with piezoelectric layers were investigated by Boroujerdy and Eslami [4, 5] in thermo-mechanical and snap-through buckling behavior utilizing the Sanders kinematic nonlinearity and classical shell theory (CST). The static and dynamic behavior of FGM circular plates under thermal-mechanical loads was studied by utilizing the central finite difference method [6] and the meshfree method combined with isogeometric analysis [7]. The Galerkin [8] and Ritz energy [9, 10] methods were used to study the FGM spherical shells and circular plates in nonlinear thermo-mechanic buckling problems. The nonlinear dynamic snap-through phenomenon was investigated by Javani et al. [11] for FGM spherical shells utilizing the generalized differential quadrature method (GDQM).

For functionally graded graphene platelet reinforced composite (FG-GPLRC) material, by employing the thermo-elastic theory of Lord-Shulman, the transient behavior of FG-GPLRC spherical shells was mentioned [12] with thermal-mechanical loads. FG-GPLRC annular plates were studied by Javani et al. [13] in the thermal buckling problem utilizing large deflection nonlinearity and FSDT. The vibration [14, 15] and thermal buckling [15] analysis of the FG-GPLRC annular plate were mentioned by utilizing principle of Hamilton and GDQM. The B-spline cubic collocation and Newmark methods combined with the Newton-Raphson method were applied to investigate the effect of the softening foundation on the nonlinear dynamic behavior of the FG-GPLRC circular plates [16]. By applying FSDT [17], and HSDT [18, 19], the thermal buckling and mechanical buckling of spherical shells and plates were mentioned using the Ritz energy method. By improving the smeared stiffener technique, stiffened FG-GPLRC spherical thin shells were also considered in the nonlinear thermo-mechanic buckling problems [20]. The vibration and dynamic buckling of FG-GPLRC circular plate and spherical shell structures subjected to electro-thermo-mechanic [21] and thermo-mechanic [22] loads were analyzed employing the functions of Euler–Lagrange to formulate the equations of motion.

To the best of the authors' knowledge, no research has focused on the dynamic thermal behavior of sandwich FG-GPLRC shallow spherical shells and circular plates with a porous core using HSDT and nonlinear viscoelastic foundation. The present paper employs the equations of Euler-Lagrange, and dissipation function of Rayleigh to derive the motion equation, incorporating the damping potential energy of the foundation. The structures are under time-dependent thermal load, and critical thermal buckling loads in both static and dynamic cases, as well as dynamic thermal buckling behavior, are analyzed. The research highlights the large effects of porosity coefficients, material properties, nonlinear foundation characteristics, and geometric parameters on the dynamic thermal buckling behavior, with findings validated through investigation.

2. Circular plates and spherical shells made of FG-GPLRC and porous core

Consider the FG-GPLRC spherical shells presented in Fig. 1, with the principal radius of shell R_0, total thickness h, base radius a_0, and the spherical coordinate system (φ, θ, z). For shallow shells, by simplifying the coordinate system to the polar coordinate system (r, θ, z) with $r = R_0 \sin\varphi$, a simpler problem can be acquired. For the FG-GPLRC circular plates, applying $R_0 \to \infty$, the governing formulations are exactly acquired.

In this study, the porous core is made of the matrix material with the thickness h_{pc}, while the external and internal FG-GPLRC face sheets are designed with the same thickness h_g. The three distributions of GPLs of external and internal face sheets are designed as [18]:

+) The external face sheets $\left(\frac{-h}{2} \le z \le \frac{-h_{pc}}{2}\right)$

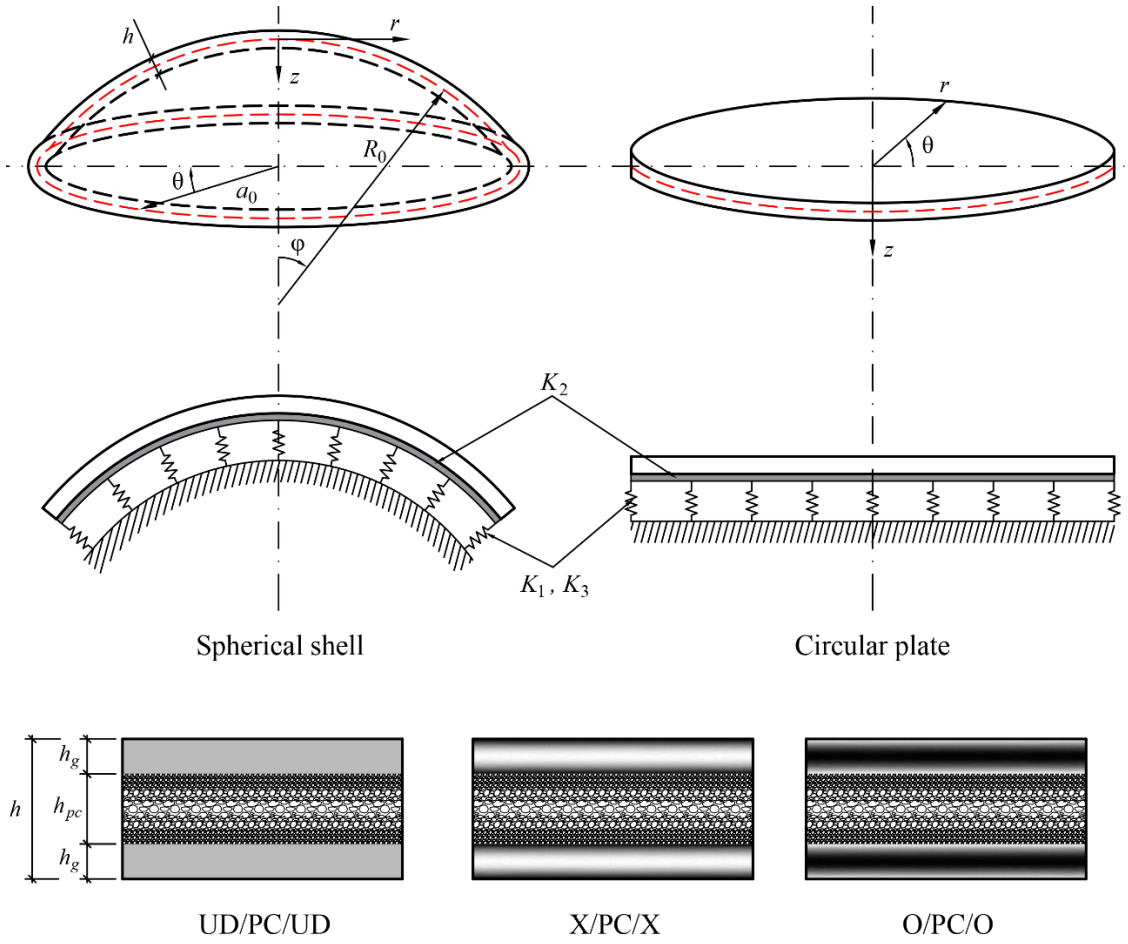

Fig. 1. Geometrical parameters, coordinate system, and material distributions of considered structures

- UD distribution:

$$\bar{W}_g = W_g, \tag{1}$$

- X distribution:

$$\bar{W}_g = \left(\left|\frac{8z + 2h + 2h_{pc}}{h - h_{pc}}\right|\right) W_g, \tag{2}$$

- O distribution:

$$\bar{W}_g = \left(2 - \left|\frac{8z + 2h + 2h_{pc}}{h - h_{pc}}\right|\right) W_g. \tag{3}$$

+) The internal face sheets $\left(\frac{h_{pc}}{2} \le z \le \frac{h}{2}\right)$

- UD distribution:

$$\bar{W}_g = W_g, \tag{4}$$

- X distribution:

$$\bar{W}_g = \left(\left|\frac{8z - 2h - 2h_{pc}}{h - h_{pc}}\right|\right) W_g, \tag{5}$$

- O distribution:

$$\bar{W}_g = \left(2 - \left|\frac{8z - 2h - 2h_{pc}}{h - h_{pc}}\right|\right) W_g, \tag{6}$$

where W_g denotes the total GPLs mass fraction.

The extended model of Halpin-Tsai is applied to predict the Young modulus of the face sheets as [19]

$$E_g = \frac{3E_m\left(1 + m_1 n_1 V_g\right)}{8\left(1 - n_1 V_g\right)} + \frac{5E_m\left(1 + m_2 n_2 V_g\right)}{8\left(1 - m_2 V_g\right)}, \tag{7}$$

where the GPLs volume fraction V_g is determined by

$$V_g = \frac{\rho_m \bar{W}_g}{\rho_m \bar{W}_g + \rho_g\left(1 - \bar{W}_g\right)}, \tag{8}$$

with the density denotes of GPLs and matrix are ρ_m and ρ_g, and

$$n_1 = \frac{\bar{E}_g - E_m}{\bar{E}_g + m_1 E_m}, \; n_2 = \frac{\bar{E}_g - E_m}{\bar{E}_g + m_2 E_m},$$

$$m_1 = \frac{2a_g}{t_g},\ m_2 = \frac{2b_g}{t_g},$$

with the matrix and GPLs moduli, length, width, and thickness of GPLs are E_m, $\bar{E}_g$, a_g, b_g, and t_g, respectively.

According to the mixture rule, the density ρ_g, thermal expansion coefficient α_g, and Poisson ratio ν_g, of the FG-GPLRC face sheets are presented as

$$\begin{aligned}\rho_g &= \left(1-V_g\right)\rho_m + \bar{\rho}_g V_g,\\ \nu_g &= \left(1-V_g\right)\nu_m + \bar{\nu}_g V_g,\\ \alpha_g &= \left(1-V_g\right)\alpha_m + \bar{\alpha}_g V_g.\end{aligned} \tag{9}$$

Effective Young's modulus, thermal expansion coefficient, and density of porous core can be estimated as [18]

$$\begin{cases} E_{pc} = E_m\left[1-e_0\cos\left(\pi z/h_{pc}\right)\right] \\ \alpha_{pc} = \alpha_m \\ \rho_{pc} = \rho_m\left[\left(\sqrt{1-e_0}-1\right)\cos\left(\pi z/h_{pc}\right)+1\right] \end{cases}, \tag{10}$$

$$-\frac{h_{pc}}{2} < z < \frac{h_{pc}}{2},$$

where e_0 $(0 \le e_0 \le 1)$ is the porosity coefficient.

With distributions of GPLs of two face sheets and the porous core (PC), three material models are acquired as O/PC/O, X/PC/X, and UD/PC/UD (Fig. 1).

By considering the thermal stresses, Hooke's law for face sheets and porous core, as

$$\begin{aligned}\begin{Bmatrix}\sigma_r \\ \sigma_\theta\end{Bmatrix} &= \begin{bmatrix}Q_{11} & Q_{12} \\ Q_{12} & Q_{22}\end{bmatrix}\left\{\begin{bmatrix}\varepsilon_r \\ \varepsilon_\theta\end{bmatrix} - \begin{bmatrix}\alpha \\ \alpha\end{bmatrix}\Delta T\right\},\\ \sigma_{rz} &= Q_{44}\varepsilon_{rz},\end{aligned} \tag{11}$$

where ΔT denotes the temperature difference between the freely thermal and the thermally stressed states and the reduced stiffnesses can be determined for FG-GPLRC face sheets as

$$Q_{11}^g = Q_{22}^g = \frac{E_g}{1-\nu_g^2},$$

$$Q_{12}^g = \frac{E_g\nu_g}{1-\nu_g^2},\quad Q_{44}^g = \frac{E_g}{2+2\nu_g}, \tag{12}$$

and for the porous core layer

$$\begin{aligned}Q_{11}^{pc} &= Q_{22}^{pc} = \frac{E_{pc}}{1-\nu_{pc}^2},\\ Q_{12}^{pc} &= \frac{E_{pc}\nu_{pc}}{1-\nu_{pc}^2},\quad Q_{44}^{pc} = \frac{E_{pc}}{2+2\nu_{pc}}.\end{aligned} \tag{13}$$

The axisymmetric displacements of sandwich FG-GPLRC structures at z coordinate can be formulated utilizing the HSDT (with $\bar{v}(r,z)=0$), as [10]

$$\begin{aligned}\bar{u}(r,z) &= z u_1(r) + u(r) - \left[w(r)_{,r} + u_1(r)\right]\frac{4z^3}{3h^2},\\ \bar{w}(r,z) &= w_0(r) + w(r),\end{aligned} \tag{14}$$

where u, v and w denote the displacements, $u_1(r)$ and $w_0(r)$ are the rotation and initial imperfect deflection.

At a distance z from the mid-surface, the strains are presented as [9]

$$\begin{aligned}\begin{Bmatrix}\varepsilon_r \\ \varepsilon_\theta \\ \varepsilon_{rz}\end{Bmatrix} &= \begin{Bmatrix}\varepsilon_r^* \\ \varepsilon_\theta^* \\ \varepsilon_{rz}^*\end{Bmatrix} + z\begin{Bmatrix}u_{1,r} \\ \dfrac{u_1}{r} \\ 0\end{Bmatrix}\\ &\quad -z^2\begin{Bmatrix}0 \\ 0 \\ \lambda\left(u_1 + w_{,r}\right)\end{Bmatrix} - z^3\begin{Bmatrix}\lambda\left(u_{1,r} + w_{,rr}\right) \\ \lambda\left(\dfrac{u_1}{r} + \dfrac{1}{r}w_{,r}\right) \\ 0\end{Bmatrix},\end{aligned} \tag{15}$$

where $\lambda = 4/3h^2$, $\varepsilon_r^*, \varepsilon_\theta^*, \varepsilon_{rz}^*$ are the mid-plane strains determined utilizing the large deflection nonlinearity, as

$$\begin{Bmatrix}\varepsilon_r^* \\ \varepsilon_\theta^* \\ \varepsilon_{rz}^*\end{Bmatrix} = \begin{Bmatrix}u_{,r} + w_{,r}w_{0,r} - \dfrac{w}{R_0} + \dfrac{1}{2}w_{,r}^2 \\ \dfrac{u}{r} - \dfrac{w}{R_0} \\ u_1 + w_{,r}\end{Bmatrix}, \tag{16}$$

By integrating Hooke's law, the forces, moments, higher-order moments, and shear forces with axisymmetric structures are formulated, as [9]

$$\begin{Bmatrix} N_r \\ N_\theta \\ M_r \\ M_\theta \\ P_r \\ P_\theta \end{Bmatrix} = \begin{Bmatrix} j_{11} & j_{12} & 0 & 0 & 0 & 0 \\ j_{12} & j_{22} & 0 & 0 & 0 & 0 \\ 0 & 0 & i_{11} & i_{12} & f_{11} & f_{12} \\ 0 & 0 & i_{12} & i_{22} & f_{12} & f_{22} \\ 0 & 0 & f_{11} & f_{12} & s_{11} & s_{12} \\ 0 & 0 & f_{12} & f_{22} & s_{12} & s_{22} \end{Bmatrix} \begin{Bmatrix} \varepsilon_r^* \\ \varepsilon_\theta^* \\ u_{1,r} \\ \dfrac{u_1}{r} \\ -\lambda\left(u_{1,r} + w_{,rr}\right) \\ -\lambda\left(\dfrac{u_1}{r} + \dfrac{1}{r} w_{,r}\right) \end{Bmatrix} - \begin{Bmatrix} \Phi_1 \\ \Phi_1 \\ 0 \\ 0 \\ 0 \\ 0 \end{Bmatrix} \Delta T, \tag{17}$$

$$\begin{Bmatrix} Q_r \\ R_r \end{Bmatrix} = \begin{Bmatrix} c_{44} & c_{45} \\ c_{45} & c_{55} \end{Bmatrix} \begin{Bmatrix} \varepsilon_{rz}^* \\ -\lambda\left(u_1 + w_{,r}\right) \end{Bmatrix},$$

where

$$\left(j_{ij}, i_{ij}, f_{ij}, s_{ij}\right) = \int_{-h/2}^{-h_{pc}/2} Q_{ij}^g \left(1, z^2, z^4, z^6\right) dz + \int_{-h_{pc}/2}^{h_{pc}/2} Q_{ij}^{pc} \left(1, z^2, z^4, z^6\right) dz + \int_{h_{pc}/2}^{h/2} Q_{ij}^g \left(1, z^2, z^4, z^6\right) dz, \quad (ij = 1, 2),$$

$$\left(s_{44}, s_{45}, s_{55}\right) = \int_{-h/2}^{-h_{pc}/2} Q_{44}^g \left(1, z^2, z^4\right) dz + \int_{-h_{pc}/2}^{h_{pc}/2} Q_{44}^{pc} \left(1, z^2, z^4\right) dz + \int_{h_{pc}/2}^{h/2} Q_{44}^g \left(1, z^2, z^4\right) dz,$$

$$\Phi_1 = \int_{-h/2}^{-h_{pc}/2} \left(Q_{11}^g + Q_{12}^g\right) \alpha_g dz + \int_{-h_{pc}/2}^{h_{pc}/2} \left(Q_{11}^{pc} + Q_{12}^{pc}\right) \alpha_{pc} dz + \int_{h_{pc}/2}^{h/2} \left(Q_{11}^g + Q_{12}^g\right) \alpha_g dz.$$

The Lagrange function is presented as

$$\Xi_{Total} = \Xi_T - \Xi_{int} + \Xi_{ext}. \tag{18}$$

The expressions of the strain energy, work done by the interaction of the foundation, and inertial energy can be determined by [21, 22]

$$\Xi_{int} = \pi \int_{-h/2}^{h/2} \int_0^{a_0} \left[\sigma_r \left(\varepsilon_r - \alpha(z)\Delta T\right) + \sigma_\theta \left(\varepsilon_\theta - \alpha(z)\Delta T\right) + \sigma_{rz}\varepsilon_{rz}\right] r dr dz, \tag{19}$$

$$\Xi_{ext} = -\pi \int_0^{a_0} \left\{\left[K_1 w - K_2\left(w_{,rr} + \frac{1}{r} w_{,r}\right) + \frac{1}{2} K_3 w^3\right] w\right\} r dr, \tag{20}$$

$$\Xi_T = \pi \int_{-h/2}^{h/2} \int_0^{a_0} \rho \ddot{\bar{w}}_{,t}^2 r dr dz, \tag{21}$$

where K_1 (N/m^3), K_2 (N/m), and K_3 (N/m^5) denote the linear Winkler and Pasternak stiffnesses, and nonlinear stiffness. The softening or hardening foundations are modeled by applying negative and positive values of K_3 .

3. Solutions and energy method

The clamped boundary conditions with axisymmetric and immovable assumptions can be presented as

$$\begin{aligned} &u = 0, \quad w = \text{finite}, u_1 = 0, \quad w_{,r} = 0 \quad \text{at } r = 0, \\ &w = 0, \quad w_{,r} = 0, \quad u_1 = 0, \quad u = 0 \quad \text{at } r = a_0, \end{aligned} \tag{22}$$

The displacement, rotation, and deflection are modeled using the polynomials satisfied the conditions (22), as [9]

$$u = U \frac{(a_0 - r)r}{a_0^2}, \quad u_1 = U_1 \frac{\left(a_0^2 - r^2\right)r}{a_0^3}, \quad w = W \frac{\left(a_0^2 - r^2\right)^2}{a_0^4}, \tag{23}$$

where U, W, U_1 are the amplitudes of displacement, deflection, and rotation,

respectively.

Similar to the deflection, the polynomial form is chosen for the imperfect deflection w_0, as

$$w_0 = \zeta h \frac{\left(a_0^2 - r^2\right)^2}{a_0^4}, \quad (24)$$

where ζ is a small imperfection size.

The damping potential function of the foundation is determined utilizing the dissipation function of Rayleigh, as

$$\Gamma = \pi \int_0^{a_0} \vartheta w_{,t}^2 r dr \quad (25)$$

By adding the dissipation function of Rayleigh, the equations of Euler–Lagrange are presented, as [21, 22]

$$\frac{d}{dt}\left(\frac{\partial \Xi_{Total}}{\partial \dot{W}}\right) - \frac{\partial \Xi_{Total}}{\partial W} + \frac{\partial \Gamma}{\partial \dot{W}} = 0,$$

$$\frac{d}{dt}\left(\frac{\partial \Xi_{Total}}{\partial \dot{U}}\right) - \frac{\partial \Xi_{Total}}{\partial U} = 0,$$

$$\frac{d}{dt}\left(\frac{\partial \Xi_{Total}}{\partial \dot{U}_1}\right) - \frac{\partial \Xi_{Total}}{\partial U_1} = 0. \quad (26)$$

leads to

$$J_{11}U + J_{13}W + J_{14}W\left(W + 2\zeta h\right) = 0, \quad (27)$$

$$J_{22}U_1 + J_{23}W = 0, \quad (28)$$

$$J_{31}U + J_{32}U_1 + J_{33}U\left(W + \zeta h\right) + J_{35}W\left(W + 4\zeta h/3\right) + J_{36}W\left(W + \zeta h\right)\left(W + 2\zeta h\right) + J_{37}K_3W^3 + J_{38}W + J_{39}\Delta T\left(W + \vartheta h\right) + J_{310}\Delta T - \frac{\pi}{5}a_0^2\left(\vartheta \dot{W} + J_{312}\ddot{W}\right) = 0, \quad (29)$$

where

$$J_{11} = -\frac{\pi\left(2j_{11} + j_{22}\right)}{6},$$

$$J_{13} = \frac{a_0\left(19j_{22} + 3j_{11} + 22j_{12}\right)\pi}{R_0},$$

$$J_{14} = \frac{\pi\left(46j_{11} - 82j_{12}\right)}{315a_0},$$

$$J_{22} = -\frac{\pi}{12}\left[\left(9c_{55}a_0^2 + 12s_{11} + 4s_{22}\right)\lambda^2 - \left(6c_{45}a_0^2 + 24f_{11} + 8f_{22}\right)\lambda + a_0^2c_{44} + 12i_{11} + 4i_{22}\right],$$

$$J_{23} = -\frac{\pi\left[\left(-3c_{55}a_0^2 - 4s_{11} - 4s_{22}/3\right)\lambda^2 + \left(2c_{45}a_0^2 + 4f_{11} + 4f_{22}/3\right)\lambda - a_0^2c_{44}/3\right]}{a_0},$$

$$J_{31} = \frac{\pi a_0\left(19j_{22} + 3j_{11} + 22j_{12}\right)}{105R_0}, \quad J_{33} = \frac{2\pi\left(-82j_{12} + 46j_{11}\right)}{315a_0},$$

$$J_{32} = -\frac{\pi\left[\left(-3a_0^2c_{55} - 4s_{11} - 4s_{22}/3\right)\lambda^2 + \left(2c_{45}a_0^2 + 4f_{11} + 4f_{22}/3\right)\lambda - c_{44}a_0^2/3\right]}{R_0},$$

$$J_{35} = \frac{4\left(j_{11} + j_{12}\right)\pi}{5R_0}, \quad J_{36} = -\frac{128\pi j_{11}}{105a_0^2}, \quad J_{37} = -\frac{\pi a_0^2}{9}$$

$$J_{38} = \frac{\pi\left[-K_1a_0^4/20 + \left(-3\lambda^2c_{55} + 2c_{45}\lambda - K_2/3 - c_{44}/3\right)a_0^2 - 4\lambda^2\left(s_{11} + s_{22}/3\right)\right]}{4a_0^2} - \frac{\pi a_0^2\left(j_{11} + 2j_{12} + j_{22}\right)}{5R_0^2},$$

$$J_{39} = 4\pi\Phi_1/3,$$

$$J_{310} = -\frac{2a_0^2\Phi_1\pi}{3R_0},$$

$$J_{312} = \int_{-h/2}^{-h_{pc}/2}\rho_g dz + \int_{-h_{pc}/2}^{h_{pc}/2}\rho_{pc}dz + \int_{h_{pc}/2}^{h/2}\rho_g dz.$$

By solving Eqs. (27) and (28), the amplitudes U and U_1 are acquired, then, substituting them into Eq. (29), leads to

$$\begin{aligned}&\left(J_{31}D_{11}+J_{32}D_{21}+J_{38}\right)W+J_{39}\Delta T\left(\zeta h+W\right)\\&+\left(J_{33}D_{11}+J_{34}D_{21}\right)W\left(\zeta h+W\right)\\&+J_{31}D_{12}W\left(2\zeta h+W\right)\\&+\left(J_{33}D_{12}+J_{36}\right)W\left(2\zeta h+W\right)\left(\zeta h+W\right)\\&+J_{37}K_3W^3+J_{35}W\left(W+4\zeta h/3\right)\\&+J_{310}\Delta T-\frac{\pi}{5}a_0^2\left(\vartheta\dot{W}+J_{312}\ddot{W}\right)=0\end{aligned}\quad(30)$$

where

$$D_{11}=-\frac{J_{13}}{J_{11}},\ D_{12}=-\frac{J_{14}}{J_{11}},\ D_{21}=-\frac{J_{23}}{J_{22}}.$$

For the perfect plates $\left(\zeta=0, R_0\to\infty\right)$, by applying $W\to 0$ in Eq. (30), the static thermal buckling temperature expression is presented by

$$\Delta T_{cr}=-\frac{J_{31}D_{11}+J_{32}D_{21}+J_{38}}{J_{39}}.\quad(31)$$

The dynamic thermal load is applied by $\Delta T=\mu t$ in this paper, where μ (K/s) is the loading speed. Eq. (30) is solved using the Runge-Kutta method, and the criterion of Budiansky-Roth is used to predict the dynamic thermal buckling loads. On the buckling region of the dynamic curve, the thermal buckling loads are chosen at the inflection point, i.e.

$$\left.\frac{d^2W}{d\Delta T^2}\right|_{\Delta T=\Delta T_{cr}}=0.\quad(32)$$

4. Results and discussions

4.1. Validation

In Table 1, the critical static buckling loads of FGM circular plates from the present results are compared with those from previous studies [1, 3, 17]. The adjacent equilibrium criterion with FSDT was used by Najafizadeh and Hedayati [1], the isogeometric finite element solutions with HSDT were applied by Loc et al. [3], and the Galerkin method, combined with FSDT, was employed by Tu et al. [17]. As observed, good agreements are achieved in these comparisons.

4.2. Numerical examples and discussions

By applying the results of Wang et al [14], the material properties of graphene platelet and cooper matrix, are acquired for the studied results in this paper.

The critical thermal buckling loads of the sandwich FG-GPLRC circular plates with porous core for static and dynamic cases are reported in Table 2. It is evident that the dynamic thermal buckling loads of the plates surpass their static ones. Furthermore, as the loading speed rises, the dynamic thermal buckling load also increases. Among the plates analyzed, the X/PC/X plate exhibits the highest thermal buckling load compared to those with other distribution plates. Table 2 highlights a notable trend: the critical thermal load changes significantly with change in porosity coefficient. Interestingly, the critical thermal buckling loads of circular plates rise as the porosity coefficient increases. This phenomenon can be explained simply. While a higher porosity coefficient decreases the stiffness of the plates, it also lowers the thermal expansion coefficient of the core, which in turn reduces the thermal edge reaction.

Fig. 2 indicates the effects of geometry, GPLs distributed models and GPLs mass fraction on the dynamic responses of plates and shells under linear time-dependent thermal loads. The region of dynamic buckling is recognized for perfect circular plates (Figs. 2a, b), and conversely for spherical shells (Fig. 2c, d). The buckling region slopes of the GPLs distributed models do not differ significantly as in Fig. 2a. The critical dynamic buckling temperatures are significantly improved as the mass fraction of GPLs increases (Fig. 2b).

Similar to Fig. 2, the dynamic thermal buckling region is recognized for perfect circular plates only (Figs. 3a and c). As can be seen, when the porosity coefficient and core thickness increase, the critical dynamic thermal buckling

temperatures and the buckling area amplitudes of the perfect plate also increase as in Figs. 3a and c. As for the spherical shell, when the porosity coefficient and core thickness increase, the dynamic thermal postbuckling strengths increase as in Fig. 3b and d.

Table 1. Validation of the critical static buckling loads ΔT_{cr} (K) of FGM circular plates

	h/a_0				
	0.05	0.04	0.03	0.02	0.01
Najafizadeh and Hedayati [1]	146.8150	94.0810	53.0290	23.6030	5.9060
Loc et al. [3]	144.9953	93.4005	52.8191	23.5719	5.9093
Tu et al. [17]	147.0435	94.4065	53.2351	23.7019	5.9318
Present	153.4901	99.1664	55.8605	24.6894	6.2178

Table 2. Dynamic critical thermal buckling load ΔT_{cr} of sandwich FG-GPLRC circular plates (K, W_g =0.5%, h =0.02m, $h_{pc} = 0.6h$, $a_0 = 20h$, ζ =0, ϑ =0 kN.s/m^3, K_1 = 10^7 N/m^3, K_2 = 10^5 N/m, K_3 = 0 MN/m^5)

Type	e_0	Static	Dynamic	
			μ = 100 (K/s)	μ = 200 (K/s)
UD/PC/UD	0	164.83	169.10	171.74
	0.3	180.26	184.80	187.44
	0.5	192.60	197.40	200.60
X/PC/X	0	165.09	169.80	172.86
	0.3	180.60	185.20	187.94
	0.5	193.00	197.40	200.00
O/PC/O	0	164.52	169.60	171.48
	0.3	179.95	184.30	188.36
	0.5	192.30	196.70	199.40

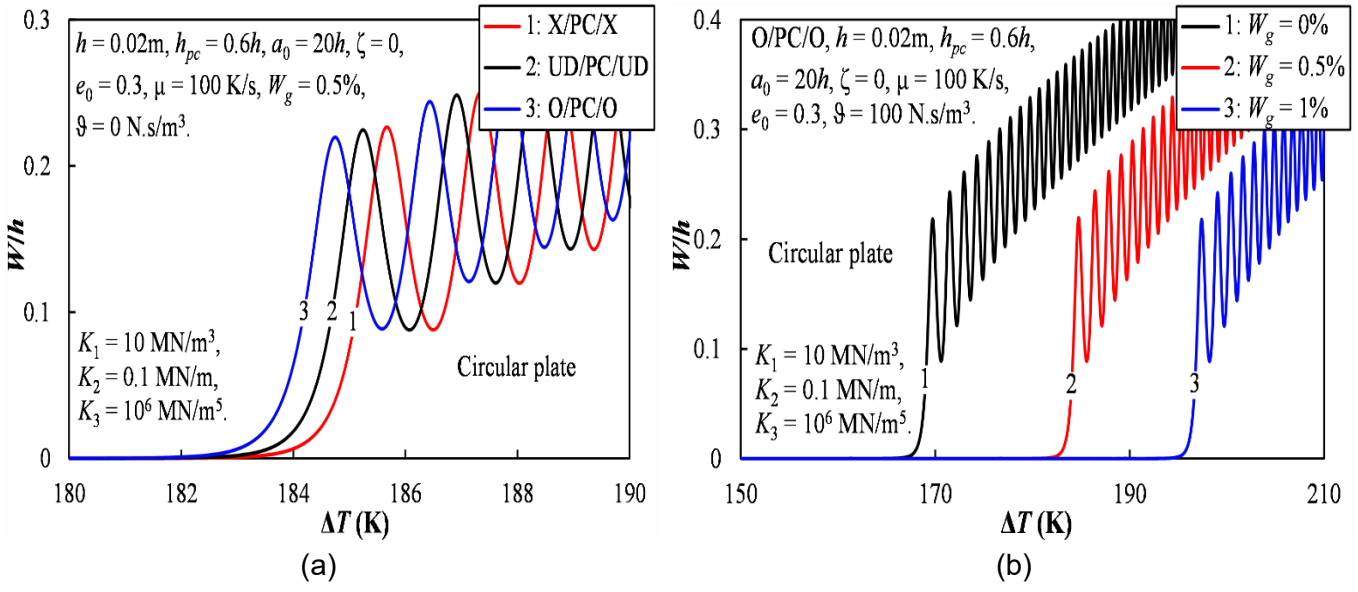

(a) (b)

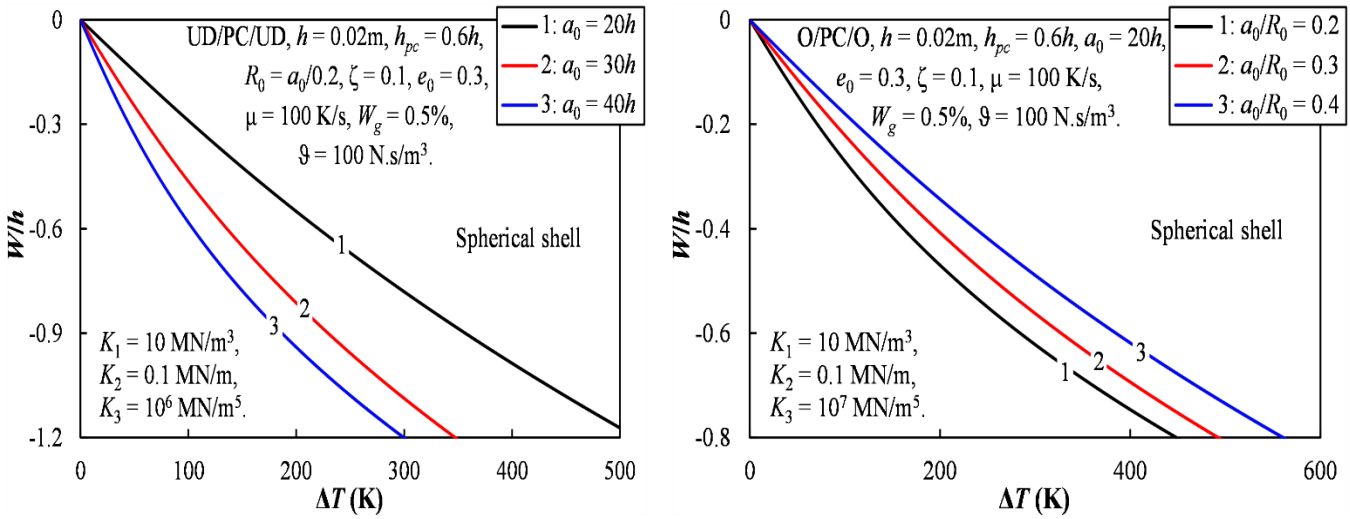

Fig. 2. Effects of geometrical, GPLs distributed models and GPLs mass fraction on the dynamic thermal responses of plates and shells under linear time-dependent thermal loads

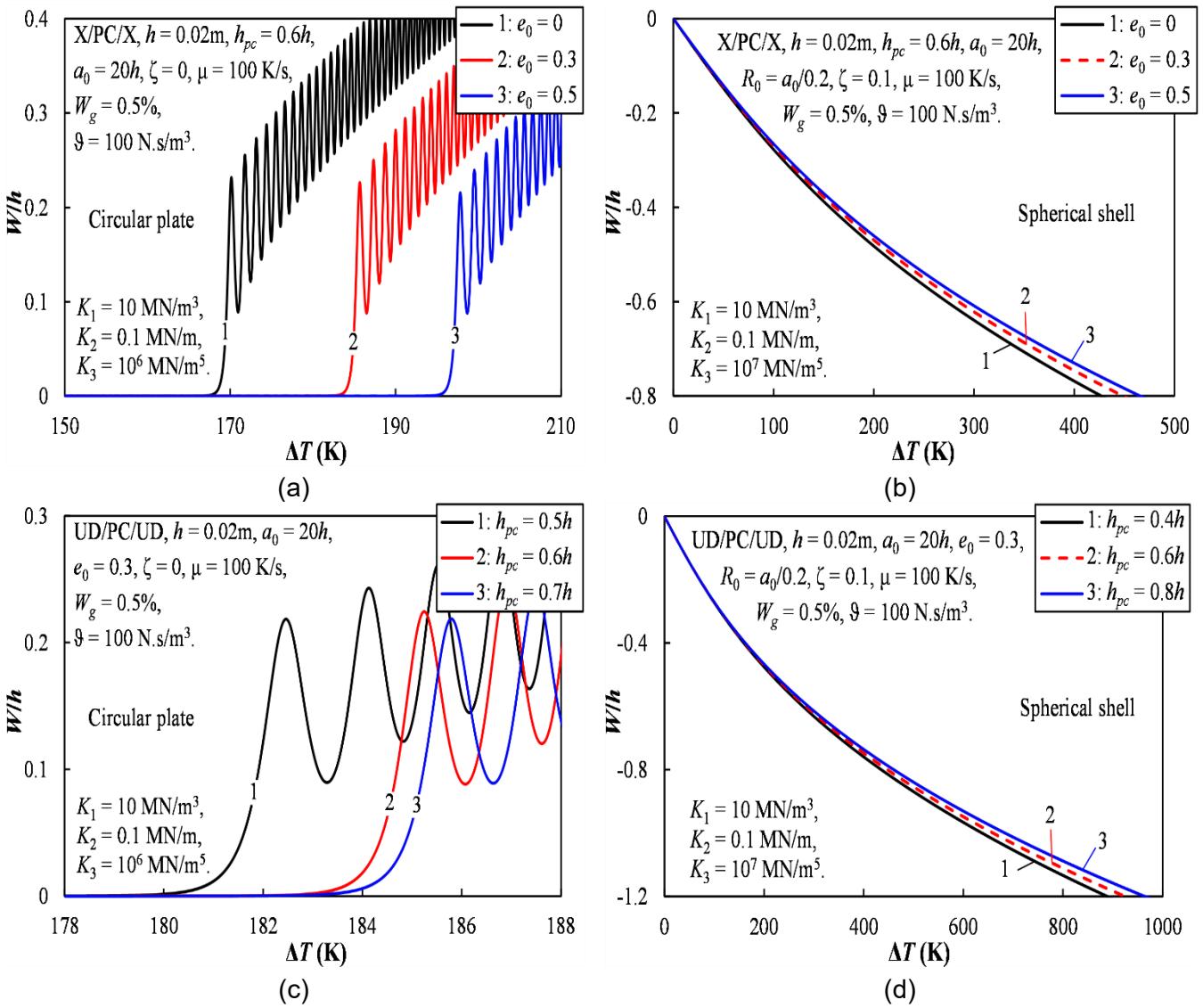

Fig. 3. Effects of core thickness and porosity coefficient on the dynamic thermal responses of plates and shells under linear time-dependent thermal loads

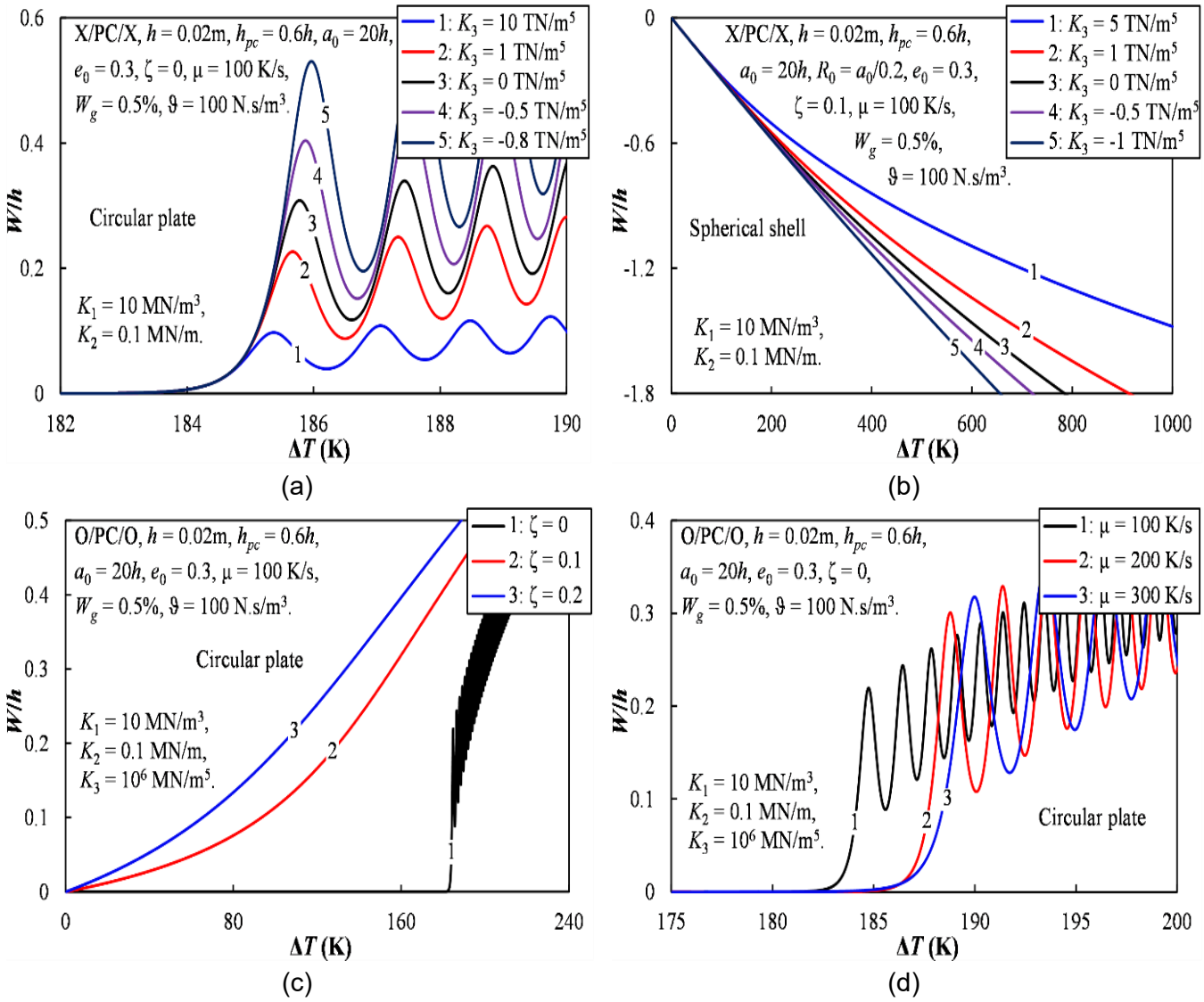

Fig. 4. Effects of the nonlinear foundation stiffness, imperfection size, and loading speed on the dynamic thermal responses of plates and shells under dynamic temperature changes

Figs. 4a and b present the effect of nonlinear foundation stiffness on the dynamic thermal responses of plates and shells. The small change in critical dynamic buckling temperature is observed corresponding with the change of nonlinear stiffness of foundation, however, the amplitude of the buckling area of the perfect plate changes significantly as in Fig. 4a. Fig. 4b shows that the dynamic thermal postbuckling strengths of the spherical shells increase gradually with positive nonlinear stiffness K_3 and decrease progressively with negative nonlinear stiffness K_3.

The effects of imperfection sizes and loading speeds on the dynamic thermal curves of the circular plates are presented in Figs. 4c and d. In Fig. 4c, as observed, the dynamic thermal buckling region is recognized with the perfect circular plate $\zeta = 0$, and oppositely for the imperfect circular plate $\zeta = 0.1, 0.2$. The critical dynamic buckling temperature and the buckling area amplitude of the plate significantly improve with larger loading speeds as shown in Fig. 4d.

5. Conclusion

The nonlinear dynamic thermal buckling behavior of the sandwich FG-GPLRC shallow spherical shells and circular plates with porous core subjected to linear time-dependent temperature changes is investigated in this paper.

The equations of motion of structures are formulated based on the Euler-Lagrange equations and HSDT. The studied results give significant points as

1) The dynamic thermal buckling region is recognized with the perfect circular plates and oppositely for the spherical shells and imperfect circular plates.
2) When the porosity coefficient and core thickness increase, the buckling area amplitude and critical dynamic thermal buckling load also increase for the perfect circular plates, and the dynamic thermal postbuckling strengths increase for the spherical shells.
3) Nonlinear foundation stiffness K_3 variations also significantly influence the dynamic thermal responses of plates and shells under linear time-dependent thermal loads.

References

[1] M.M. Najafizadeh, B. Hedayati. (2004). Refined theory for thermoelastic stability of functionally graded circular plates. *Journal of Thermal Stresses*, 27(9), 857-880.

[2] T. Prakash, M. Ganapathi. (2006). Asymmetric flexural vibration and thermoelastic stability of FGM circular plates using finite element method. *Composites Part B: Engineering*, 37(7-8), 642-649.

[3] T.V. Loc, T.H. Chien, H. Nguyen-Xuan. (2013). An isogeometric finite element formulation for thermal buckling analysis of functionally graded plates. *Finite Elements in Analysis and Design*, 73, 65-76.

[4] M.S. Boroujerdy, M.R. Eslami. (2013). Nonlinear axisymmetric thermomechanical response of piezo-FGM shallow spherical shells. *Archive of Applied Mechanics*, 83, 1681-1693.

[5] M.S. Boroujerdy, M.R. Eslami. (2014). Axisymmetric snap-through behavior of Piezo-FGM shallow clamped spherical shells under thermo-electro-mechanical loading. *International Journal of Pressure Vessels and Piping*, 120-121, 19-26.

[6] Y. Kiani. (2017). Axisymmetric static and dynamics snap-through phenomena in a thermally postbuckled temperature-dependent FGM circular plate. *International Journal of Non-Linear Mechanics*, 89, 1-13.

[7] P. Tan, N.T. Nhon, T. Rabczuk, K. Zhou. (2018). Static, dynamic and buckling analyses of 3D FGM plates and shells via an isogeometric-meshfree coupling approach. *Composite Structures*, 198, 35-50.

[8] V.T. Long, H.V. Tung. (2023). Postbuckling responses of porous FGM spherical caps and circular plates including edge constraints and nonlinear three-parameter elastic foundations. *Mechanics Based Design of Structures and Machines*, 51(8), 4214-4236.

[9] L.N. Ly, D.T.N. Thu, D.T. Dong, V.M Duc, B.T. Tu, N.T. Phuong, V.H. Nam. (2023). A Novel Analytical Approach for Nonlinear Thermo-Mechanical Buckling of Higher-Order Shear Deformable Porous Circular Plates and Spherical Caps with FGM Face Sheets. *International Journal of Applied Mechanics*, 15(05), 2350035.

[10] B.T. Tu, D.T. Dong, V.M Duc, V.H. Nam. (2024). Nonlinear Buckling and Postbuckling Response of Porous FGM Shallow Spherical Caps and Circular Plates with Nonlinear Elastic Foundation Effects Using the Ritz Energy Method. *Mechanics of Composite Materials*, 60, 417-432.

[11] M. Javani, Y. Kiani, M.R. Eslami. (2024). Nonlinear dynamic response of a temperature-dependent FGM spherical shell under various boundary conditions and thermal shocks: Examination of dynamic snap-through. *Thin-Walled Structures*, 199, 111796.

[12] Y. Heydarpour, P. Malekzadeh, F. Gholipour. (2019). Thermoelastic analysis of FG-GPLRC spherical shells under thermo-mechanical loadings based on Lord-Shulman theory. *Composites Part B: Engineering*, 164,

400-424.

[13] M. Javani, Y. Kiani, M.R. Eslami. (2020). Thermal buckling of FG graphene platelet reinforced composite annular sector plates. *Thin-Walled Structures*, 148, 106589.

[14] Y. Wang, R. Zeng, M. Safarpour. (2020). Vibration analysis of FG-GPLRC annular plate in a thermal environment. *Mechanics Based Design of Structures and Machines*, 50(1), 352-370.

[15] Y. Yang, B. Chen, W. Lin, Y. Li, Y. Dong. (2021). Vibration and symmetric thermal buckling of asymmetric annular sandwich plates with piezoelectric/GPLRC layers rested on foundation. *Aerospace Science and Technology*, 110, 106495.

[16] Z. Dai, H. Tang, S. Wu, M. Habibi, Z. Moradi, H.E. Ali. (2023). Nonlinear consecutive dynamic instabilities of thermally shocked composite circular plates on the softening elastic foundation. *Thin-Walled Structures*, 186, 110645.

[17] B.T. Tu, L.N. Ly, N.T. Phuong. (2022). A new analytical approach of nonlinear thermal buckling of FG-GPLRC circular plates and shallow spherical caps using the FSDT and Galerkin method. *Vietnam Journal of Mechanics*, 44(4), 418-430.

[18] L.N. Ly, D.T.N. Thu, D.T. Dong, V.M. Duc, N.T. Phuong. (2023). Nonlinear thermo-mechanical buckling and postbuckling of sandwich FG-GPLRC spherical caps and circular plates with porous core by using higher-order shear deformation theory. *Journal of Thermoplastic Composite Materials*, 36(10), 4083-4105.

[19] N.T. Phuong, D.T. Dong, B.T. Tu, V.M. Duc, L.N. Khuong, P.T. Hieu, V.H. Nam. (2024). Nonlinear thermo-mechanical axisymmetric stability of FG-GPLRC spherical shells and circular plates resting on nonlinear elastic medium. *Ships and Offshore Structures*, 19(6), 820-830.

[20] V.H. Nam, T.Q. Minh, P.T. Hieu, V.T. Hung, B.T. Tu, N.T.T. Hoai, D.T. Dong. (2023). A new analytical approach for nonlinear thermo-mechanical postbuckling of FG-GPLRC circular plates and shallow spherical caps stiffened by spiderweb stiffeners. *Thin-Walled Structures*, 193, 111296.

[21] V.H. Nam, P.N. Nam, B.T. Tu, V.M. Duc, N.T. Phuong. (2024). A new semi-analytical approach for nonlinear electro-thermo-mechanical dynamic responses of FG-GPLRC shallow spherical caps and circular plates with porous core. *Journal of Thermoplastic Composite Materials*. DOI: 10.1177/08927057241259760.

[22] B.T. Tu, V.M. Duc, P.N. Nam, C.V. Doan, V.H. Nam. (2024). Nonlinear thermo-mechanical dynamic buckling and vibration of FG-GPLRC circular plates and shallow spherical shells resting on the nonlinear viscoelastic foundation. *Archive of Applied Mechanics*, 94(12), 3715-3729. DOI: 10.1007/s00419-024-02691-6.